coatings

MDPI

Article

Effect of Impurities Spacing on Fatigue Strength Coefficient

Tomasz Lipiński

Department of Material and Machine Technology, The Faculty of Technical Sciences, University of Warmia and Mazury in Olsztyn, 10-719 Olsztyn, Poland; tomekl@uwm.edu.pl

Abstract: The influence of impurities present in steel on fatigue strength has been the subject of research conducted for many years. Despite a large number of studies, there is no unambiguous explanation of the influence of impurities on the fatigue life of steel. The interpretation of the results becomes more complicated as the ductility of the steel increases. For this reason, most of the research concerns low-ductility hard steels. In addition, the studies presented in the literature mostly concern laboratory conditions, which the authors of the papers have tried (with varying degrees of success) to adapt to industrial research. There are a few studies on the influence of impurities in steel on the fatigue resistance factor. The coefficient *k* is the result of the fatigue strength *zg* divided by the hardness of the steel. With its help, it is possible to determine the fatigue strength depending on the hardness of the steel. In the presented work, an attempt was made to determine the impact of impurities of different sizes and located at different distances from each other on the fatigue strength coefficient. The analysis was carried out at seven heats made in industrial conditions. Melting was carried out in electric furnaces with a capacity of 140 tons. Steel from all melts was subjected to desulfurization. Samples with a diameter of 18 mm were taken. The samples were hardened from the austenitizing temperature of 880 °C. To diversify the microstructure and mechanical properties, the steel was tempered at temperatures from 200 to 600 °C. After heat treatment, the samples were subjected to rotational bending. Based on the tests, it was found that the fatigue strength coefficient *k* depends on the size of the impurities and the distance between the inclusions. A difference in the specific k-factors was noted depending on the microstructure of the steel.

Keywords: steel; high-quality steel; fatigue strength; fatigue strength coefficient; inclusions in steel

Citation: Lipiński, T. Effect of Impurities Spacing on Fatigue Strength Coefficient. *Coatings* **2023**, *13*, 242. https://doi.org/10.3390/coatings13020242

Academic Editor: Paolo Castaldo

Received: 27 December 2022
Revised: 17 January 2023
Accepted: 18 January 2023
Published: 20 January 2023

1. Introduction

Steel is currently one of the most popular construction materials. Its microstructure determines its functional properties, and therefore its application. The properties of steel depend on many, often interrelated, factors. These include the chemical composition, widely understood method of production, heat treatment, etc. [1–6]. Impurities have a large impact on the mechanical properties of high-quality steel and the role of impurities in steel may be different [7–10]. It depends on the type, size, shape of the impurities, and the distribution of the inclusions, but also on the structure of the steel, which is their matrix of impurities. Unfortunately, non-metallic impurities mainly play a negative role [11–17].

Despite the research conducted for many years to improve the manufacturing processes, it has not been possible to eliminate non-metallic inclusions from the steel microstructure. Their almost complete elimination is expensive and very difficult to achieve in industrial conditions. In practice, the pursuit of the complete elimination of impurities in most metal alloys is unjustified both in economics and in terms of their material properties. Usually, the impurity content in steel is small, but their influence on the technological and strength properties, especially fatigue life and fatigue strength, is significant [18–22].

The tendency to form and then develop micro-cracks during variable loads are the factors determining the fatigue life of the material [23–25]. Therefore, an important role in shaping the properties of the construction material is played by the dimensional structure of the inclusions in connection with its distribution. The placement of non-metallic

inclusions is also important [26–30]. A single inclusion has a different effect than a cluster of inclusions. Additionally, the distance between impurities can affect the properties of the steel. Assuming a constant volume of impurities in the steel, small distances mean the presence of a large amount of fine impurities, while large distances mean the presence of a small amount of impurities, but of large dimensions. Non-metallic inclusions may cause inconsistencies at the precipitation-matrix interface during plastic processing and heat treatment. The quality, quantity, size, geometric shape, and distribution of impurities in the steel microstructure also depend on the production process [31–39].

The possibility of micro-crack formation, and then the speed of their growth, but also the amount of stresses in the steel that may affect the fatigue life of the elements, may be caused by the resistance encountered by dislocations moving in the material. This resistance can be measured by the hardness or tensile strength of the steel. A solution to the problem is also sought by considering local stresses and deformations in the steel microstructure, formation, joining, and development of microcracks [40–42]. Many papers have presented the results of studies on the impact of non-metallic inclusions on the fatigue properties of hard matrix steels, for example, bearing steels [43–46].

A solution to the problem is also sought by considering the local stresses and strains in the steel microstructure, nucleation, and the development and joining of microcracks. For a full analysis of the issue, it is necessary to consider the behavior not only of the inclusions themselves and their morphology, but also in connection with the impurity matrix, which is the steel microstructure [47–52]. Many papers have presented the results of studies on the impact of impurities on the fatigue properties of hard matrix steels, for example, bearing and small-volume steels. There are not many studies analyzing the durability of steels with a low carbon content and high ductility. These shortcomings also confirm the desirability of the analysis presented in this paper. Conducting fatigue strength tests is time-consuming and expensive, especially for melts carried out on an industrial scale. For these reasons, computer simulations are increasingly carried out in practice [53,54]. These simulations try to reflect the material manufacturing conditions. However, in order to be able to simulate industrial production, they should be carried out on the basis of data obtained in industrial conditions. There are known models and equations that allow one to determine the fatigue strength as a function of strength from a static tensile test. Because Equation (1) [55]:

$$z_g = m \cdot R_m, \tag{1}$$

and Equation (2)

$$R_m = n \cdot HV, \tag{2}$$

then replacing the coefficients m and n with the coefficient k in Equation (3)

$$k = z_g \cdot HV^{-1}, \tag{3}$$

where:

z_g—fatigue strength, MPa;
m—coefficient of the equation compares the fatigue strength with the static strength;
n—coefficient of the equation compares the tensile strength with hardness;
R_m—tensile strength, MPa;
HV—Vickers hardness, MPa;
k—fatigue strength coefficient.

In industrial practice and for better adaptation of computer programs to determine the fatigue strength coefficient, on the basis of knowledge of other parameters, stereological parameters are also used. Many papers have been devoted to the analysis of impurities present in steel and its fatigue strength. However, only a few papers in the literature have analyzed the effect of impurities present in industrially produced steel on the factor k described by Equation (3). An analysis based on an experiment performed in real conditions on an industrial scale (presented in this paper) is necessary to correctly relate the fatigue strength to hardness under assumed conditions, particularly at a certain content of

impurities. Determination of the k coefficient on the basis of the conducted industrial tests enables a quick and cheap estimation of the fatigue strength of steel based on the impurity spacing and microstructure, which can represent the tempering temperature.

The main aim of the paper was to determine the fatigue strength coefficient of steel with different microstructures depending on the size and average distance between the impurities.

2. Materials and Methods

In order to obtain data that could perfectly reflect the industrial conditions, the tests were carried out on steel heated in industrial conditions. The tests were carried out on steel classified as low-carbon steel, although the carbon content of the tested steel lies on the border of low-carbon and medium-carbon steel. In order to enable the analysis of the impact of impurities contained in the microstructure matrix of different hardness and ductility, the steel was subjected to heat treatment consisting of hardening and low, medium, and high tempering. High purity steel weighing 140 tons was heated in an electric furnace. For seven independent heats, pig iron with the addition of about 25% of steel scrap was used each time. After each heating, the metal was lowered into a seven-ton ladle. Each of the heats was subjected to desulfurization. After the metal crystallization process, billets of 100 mm × 100 mm were rolled using traditional methods.

Sections were taken from the rolled billets for the analysis of the chemical composition of steel, microscopic examination, and quantitative and qualitative analysis of the impurities in the form of oxide inclusions. The chemical composition of steel was tested using the AFL FICA quantometer, LECO analyzers, and classical chemistry. The volume of impurities on the surface of the metallographic microsection was divided into groups of sizes from: 2 µm, 5 µm, 10 µm, 15 µm, 25 µm, 35 µm, and 45 µm was assessed at 400× magnification using the Quantimet video microscope. The real relative volume of inclusions was determined using chemical extraction methods. The volume of particles with a size of less than 2 µm was the difference between the total volume of inclusions and the volume of impurities with a size of 2 µm and larger. During the analysis of the test results, it was found that the volume of impurities of the Me–S type was below the limit value of the determination error. It was also the basis for omitting Me–S type inclusions from further analysis. Non-metallic inclusions of the Me–O type were subjected to further analysis.

The real average chemical composition of the tested steel and its standard deviation from seven heats is presented in Table 1.

Table 1. Average chemical composition and standard deviation of the tested steel from seven heats (wt. %).

Chemical Element	C	Mn	Cr	Ni	Mo	Si	Cu	P	S	B
Contents	0.26	1.18	0.52	0.50	0.25	0.24	0.15	0.02	0.01	0.003
Standard deviation	0.03	0.19	0.03	0.04	0.02	0.07	0.04	0.003	0.003	0.001

Cylindrical samples with a diameter of 10 mm with symmetry axes arranged parallel to the direction of plastic working were taken from 100 mm × 100 mm billets. Test samples were prepared in accordance with the standards of PN-H/74-04327:1974 [56]. Next, the samples were hardened from the temperature of 880 °C. After hardening, the samples were tempered and cooled in air. The fatigue strength test was carried out on 73 samples tempered at 200 °C, 75 at 300 °C, 71 at 400 °C, 73 at 500 °C, and 74 at 600 °C.

The fatigue strength of the steel was determined on the VEB Werkstoffprufmaschinen rotary bending fatigue strength test machine. The rotational bending speed was 6000 rpm. Two-sided rotating handles were used. The research were carried out based on the PN-74/H-04327 standard. The samples were bent to breakage or to 10^7 cycles. The load on the samples during the tests was selected experimentally based on the initial fatigue strength and then the load was made dependent on the tempering temperature of the steel. The

applied load guaranteed a minimum durability of 10^4 cycles. The following loads were applied to the rotationally bent samples: 650 MPa for a tempering temperature of 200 °C, 600 MPa for 300 °C, 600 MPa for 400 °C, 600 MPa for 500 °C, and 540 MPa for 600 °C.

The arithmetic average distances between non-metallic inclusions $\overline{\lambda}$ were calculated using the following Formula (4):

$$\overline{\lambda} = \frac{2}{3}\overline{d}\left(\frac{1}{V} - 1\right) \quad (4)$$

where:

$\overline{d}$—average diameter of impurity, µm,

V—relative volume of non-metallic inclusions, %.

The fatigue strength coefficients determined for the tested steel depending on the tempering temperatures were presented in the general form of Equation (5):

$$k_{(tempering\ temperature)} = a \cdot \lambda + b, \quad (5)$$

where:

$k_{(tempering\ temperature)}$—fatigue strength coefficient depending on the tempering temperature;

a, b—coefficients of the equation;

λ—impurities spacing, µm.

The significance of the regression equation represented by the correlation coefficients r was checked based on the distribution of the Student's t function for $\alpha = 0.05$ and the degrees of freedom $f = n - 1$.

The scattering coefficient $\delta(tempering\ temperature)$ for the regression equation $k(tempering\ temperature)$ was calculated by Equation (6):

$$\delta_{(tempering\ temperature)} = \frac{2 \cdot s}{\sqrt{1 - r^2}} \quad (6)$$

where:

s—standard deviation;

r—correlation coefficient.

3. Results

The microstructures of the researched steel after hardening at 880 °C and tempering at different temperatures from 200 °C to 600 °C are presented in Figure 1: 1a—low tempered martensite, 1b—medium tempered martensite, 1c—medium tempered martensite with cementite formations, 1d—sorbitol, 1f—spheroidite.

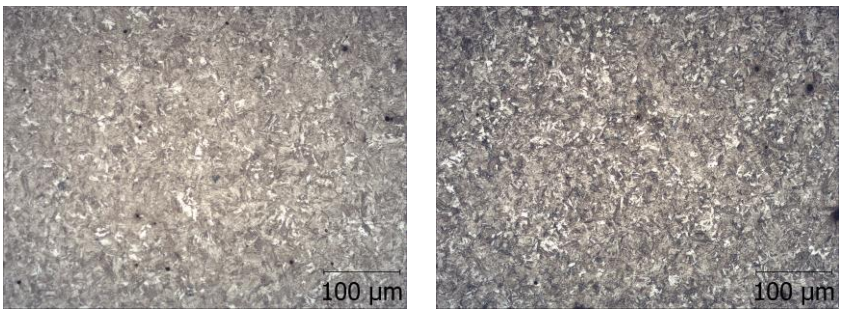

(**a**) (**b**)

Figure 1. *Cont.*

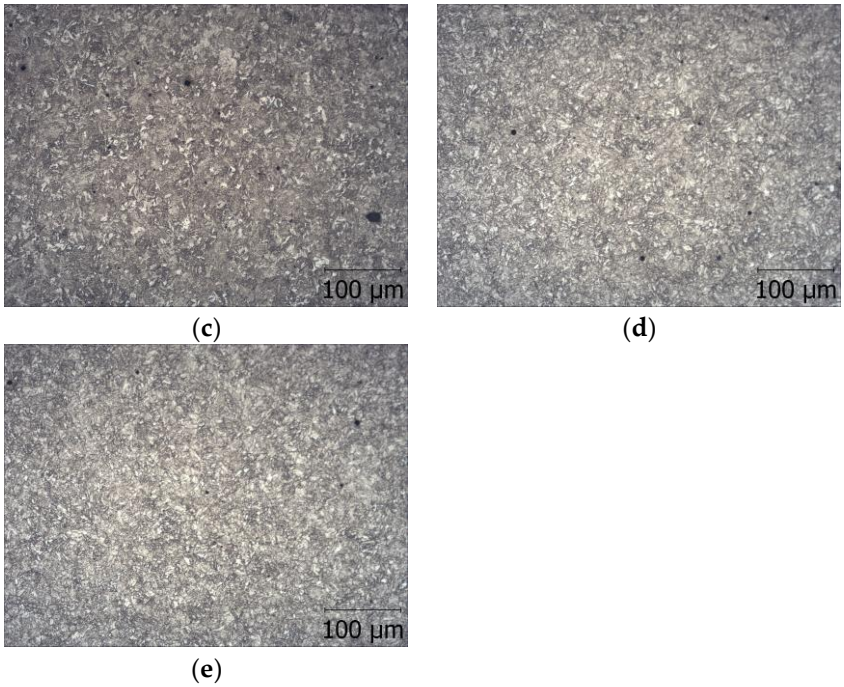

(**c**) (**d**)

(**e**)

Figure 1. Microstructure of the tested steel after being hardened at 880 °C and tempered at (**a**) 200 °C, (**b**) 300 °C, (**c**) 400 °C, (**d**) 500 °C, and (**e**) 600 °C.

An exemplary distribution of non-metallic inclusions in individual dimensional ranges for one of the heats is shown in Figure 2.

Exemplary results of the qualitative and quantitative analysis of non-metallic inclusions for one of the melts carried out using XRD are shown in Figure 3.

The fatigue strength coefficient determined for rotational bending k of the tested steel after hardening at 880 °C and tempering at 200 °C, depending on the size and spacing of impurities λ, is shown in Figure 4.

The regression equation with correlation coefficient r of the tested steel after hardening from 880 °C and tempering at 200 °C are presented in Equation (7).

$$k_{(200)} = -0.0251 \cdot \lambda + 0.911 \text{ and } r = 0.9545 \quad (7)$$

The fatigue strength coefficient determined for rotational bending k of the tested steel after hardening at 880 °C and tempering at 300 °C, depending on the size and spacing of impurities λ, is shown in Figure 5.

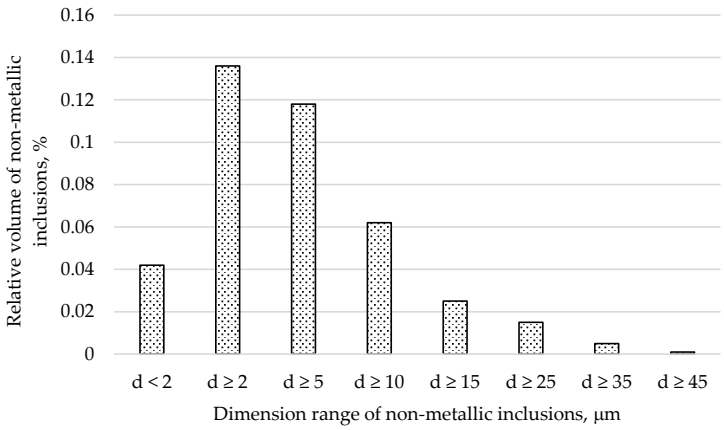

Figure 2. An exemplary distribution of non-metallic inclusions in individual dimensional ranges in the tested steel.

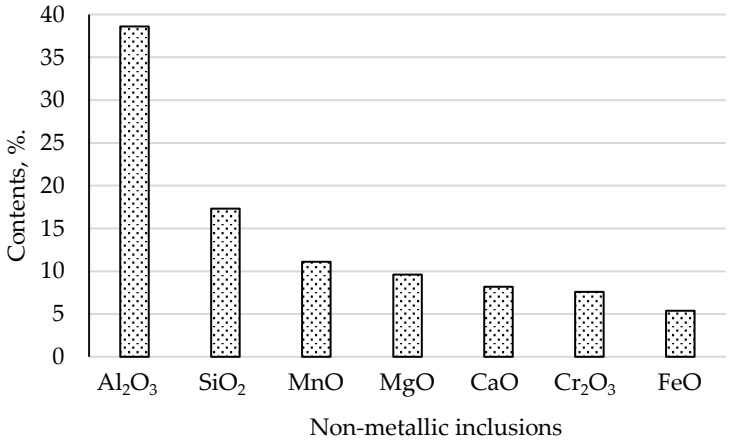

Figure 3. Exemplary results of the qualitative and quantitative analysis of non-metallic inclusions in the tested steel.

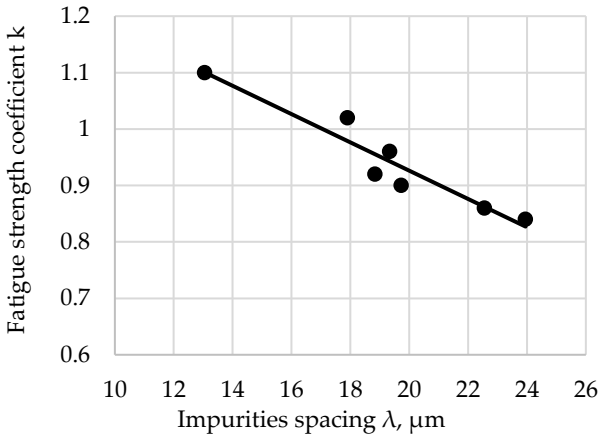

Figure 4. Fatigue strength coefficient, *k*, of tested steel after hardening from 880 °C and tempering at 200 °C depends on the impurities spacing λ.

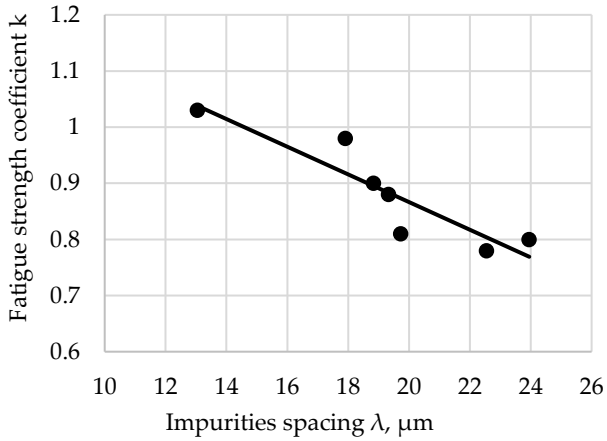

Figure 5. Fatigue strength coefficient, *k*, of the tested steel after hardening from 880 °C and tempering at 300 °C depends on the impurities spacing λ.

Regression equation with correlation coefficient *r* of the tested steel after hardening from 880 °C and tempering at 300 °C are presented in Equation (8).

$$k_{(300)} = -0.0247 \cdot \lambda + 1.3539 \text{ and } r = 0.9087 \quad (8)$$

The fatigue strength coefficient determined for rotational bending k of the tested steel after hardening at 880 °C and tempering at 400 °C, depending on the size and spacing of impurities λ, is shown in Figure 6.

Regression equation with correlation coefficient r of the tested steel after hardening from 880 °C and tempering at 400 °C is presented in Equation (9).

$$k_{(400)} = -0.0255 \cdot \lambda + 1.4253 \text{ and } r = 0.8023 \quad (9)$$

The fatigue strength coefficient determined for rotational bending k of the tested steel after hardening at 880 °C and tempering at 500 °C, depending on the size and spacing of impurities λ, is shown in Figure 7.

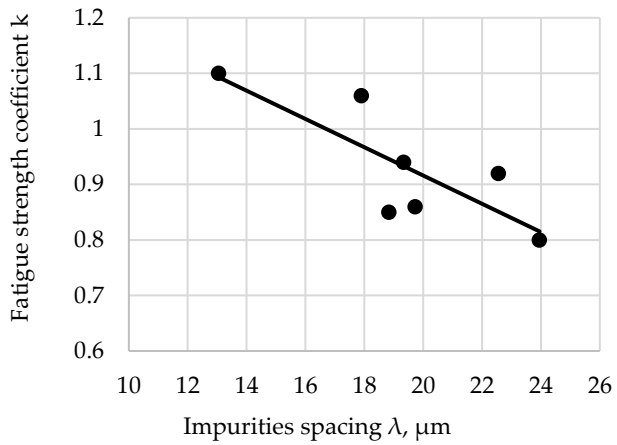

Figure 6. Fatigue strength coefficient, k, of the tested steel after hardening from 880 °C and tempering at 400 °C depends on impurities spacing λ.

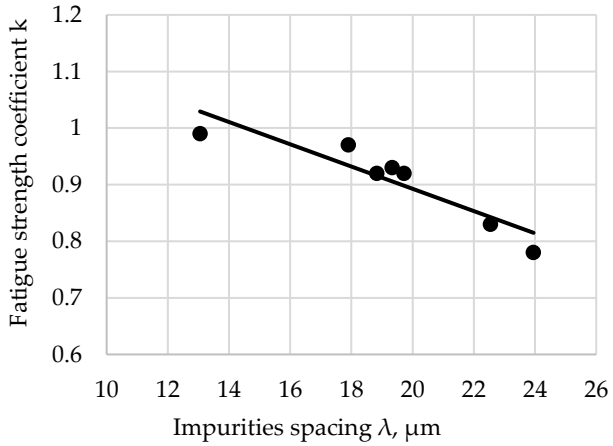

Figure 7. Fatigue strength coefficient, k, of the tested steel after hardening from 880 °C and tempering at 500 °C depends on impurities spacing λ.

Regression equation with the correlation coefficient r of the tested steel after hardening from 880 °C and tempering at 500 °C are presented in Equation (10).

$$k_{(500)} = -0.0197 \cdot \lambda + 1.286 \text{ and } r = 0.9180 \quad (10)$$

The fatigue strength coefficient determined for rotational bending k of the tested steel after hardening at 880 °C and tempering at 600 °C, depending on the size and spacing of impurities λ, is shown in Figure 8.

Regression equation with correlation coefficient r of the tested steel after hardening from 880 °C and tempering at 600 °C are presented in Equation (11).

$$k_{(600)} = -0.0212 \cdot \lambda + 1.3078 \text{ and } r = 0.8480 \quad (11)$$

The fatigue strength coefficient determined for rotational bending *k* of the tested steel after hardening at 880 °C and tempering at all tempering temperatures, depending on the size and spacing of impurities λ, is shown in Figure 9.

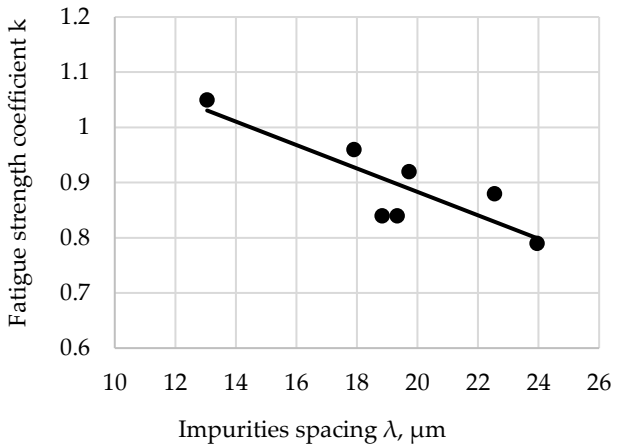

Figure 8. Fatigue strength coefficient, *k*, of the tested steel after hardening from 880 °C and tempering at 600 °C depends on impurities spacing λ.

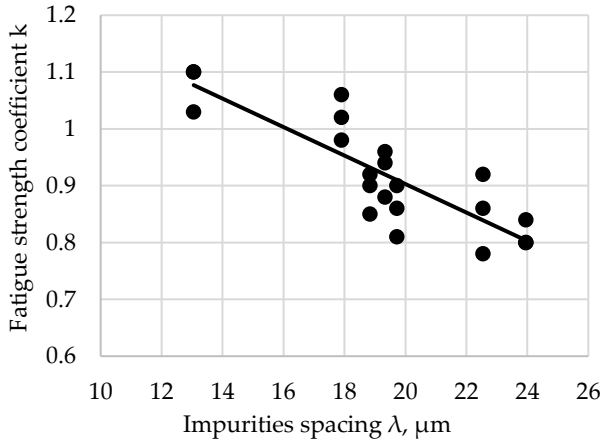

Figure 9. Fatigue strength coefficient, *k*, of the tested steel after hardening from 880 °C and tempering for all tempering temperatures depends on impurities spacing λ.

Regression equation with correlation coefficient *r* of the tested steel after hardening from 880 °C and tempering at all tempering temperatures is presented in Equation (12).

$$k_{(all)} = -0.0251 \cdot \lambda + 1.4041 \text{ and } r = 0.8454 \quad (12)$$

The statistical parameters for the mathematical model (5), correlation coefficients, and the degree of dissipation, *k*, around the regression line are presented in Table 2.

Table 2. Statistical parameters representing mathematical Equation (5), correlation coefficients, and dissipation (6).

Tempering Temperature °C	Correlation Coefficient r	Degree of Dissipation, δ (6), Around Regression Line (5)	$t_\alpha = 0.05$	$t_\alpha = 0.05$ from Student's Distribution for $p = (n - 1)$
200	0.9545	0.0867	7.8402	
300	0.9087	0.0605	5.3320	
400	0.8023	0.1828	3.2923	2.4469
500	0.918	0.0811	5.6701	
600	0.848	0.1048	3.9192	
all	0.8454	0.1238	9.2289	2.0452

4. Discussion of the Research Results

The steel analyzed in this paper contained an average of 0.26% C with a standard deviation of 0.03% (Table 1). Taking into account the traditional division of steel in terms of the limiting carbon content into low-carbon (up to 0.25% C) and medium-carbon (above 0.25% C), it can be concluded that this steel lies on the border of low-carbon and medium-carbon steel. Hardening and tempering carried out at different temperatures resulted in the diversification of the microstructure as well as the microstructure-related properties of the steel. Microstructures of low, medium, and high tempered martensite were obtained. The analysis of the share of non-metallic inclusions in steel (Figure 2) indicates the highest content of impurities above 2 μm. The share of impurities considered in the literature to be large above 10 μm was much smaller and constituted about 0.06% of the steel volume. This proves the high purity of the tested material. Quite a high content of impurities was found for the dimensional range below 2 μm. Their share in the volume of steel was about 0.04%, but considering their size, one should expect a large number of these inclusions. On the basis of the XRD analysis, it was found that the highest number of Al_2O_3 inclusions was found in the tested steel. For the analyzed melt, their volume was determined to be about 39% of the volume of all impurities. Much smaller shares were found for other impurities (e.g., about: 18% SiO_2, 11% MnO). Other groups of pollutants were below 10% (Figure 3).

By analyzing the fatigue strength coefficient of steel as a function of the size and impurities spacing λ for individual variants of heat treatment represented by the tempering temperatures, it was found that the fatigue strength decreased with the increase in λ (Figures 4–8). A similar relationship was also noted simultaneously for the compilation of results for all tempering temperatures (Figure 9). It should be emphasized that this effect was achieved for steel melted in industrial conditions, but still of high purity. In addition, it should be taken into account that the tested steel contained a large number of small inclusions. It should also be noted that all of the presented Equations (7)–(12) had high statistical significance, which was confirmed by the analysis of Table 2. Analyzing parameter (5) of the regression Equations (7)–(12), a negative slope was found in all equations. This means that as the value of λ increases, the values of k decrease. High coefficient correlations among all variants were obtained for hard steels after tempering at 200 and 300 °C. Low dispersion coefficients were also obtained for the same parameters. For the fatigue strength tests, a random distribution of cracks in the tested samples should be assumed. Nevertheless, it can be concluded with high probability that the fatigue strength coefficient decreases with the increase in λ. Such a consideration is consistent with the theory known from the literature, according to which large impurities reduce the fatigue strength of steel. In the discussed results, the increase in impurities spacing in connection with the size of non-metallic inclusions λ (4), assuming a constant value of the volume of impurities in the microstructure, is directly proportional to the size of the impurities. Thus, when λ is greater, non-metallic inclusions with larger dimensions should be expected. Large inclusions, on the other hand, cause a reduction in fatigue strength, and thus the k-coefficient. Analyzing the obtained test results and comparing them with

the results of other papers, it is necessary to indicate the need for further research on fine inclusions. These inclusions, due to their small volume and thus low energy, should take forms similar to spheroids. This may cause an increase in the stacking error energy and thus enable the slip to be activated, mainly with materials capable of plastic deformation. A completely different mechanism is to be expected from large inclusions. They will have a large volume (larger than 10 μm), and therefore energy that may favor the formation of larger precipitates. In addition, large precipitates will have a greater ability to crack, which may result in a reduction in the analyzed coefficient *k*.

5. Conclusions

The research carried out on an industrial scale allowed for:

1. Determination of the fatigue strength coefficient taking into account non-metallic inclusions for different tempering temperatures;
2. Analysis of the size and impurities spacing of non-metallic inclusions for different tempering temperatures;
3. Showing that the fatigue strength coefficient can be represented with a sufficiently high accuracy in the form of a single equation for all tempering temperatures;
4. Indication of the area of future work, namely, the impact of fine particles on the fatigue strength parameters of steel.

Funding: This research received no external funding.

Institutional Review Board Statement: Not applicable.

Informed Consent Statement: Not applicable.

Data Availability Statement: Not applicable.

Conflicts of Interest: The authors declare no conflict of interest.

References

1. Scorza, D.; Carpinteri, A.; Ronchei, C.; Vantadori, S.; Zanichelli, A. A novel methodology for fatigue assessment of high strength steels with non-metallic inclusions. *Procedia Struct. Integr.* **2022**, *39*, 503–508. [CrossRef]
2. Jopek, M. Determination of Carbon Steel Dynamic Properties. *Manuf. Technol.* **2021**, *21*, 479–482. [CrossRef]
3. Suresh, S. *Fatigue of Materials*; Cambridge University Press: Cambridge, UK, 1998.
4. Kováčiková, P.; Dubec, A.; Kuricová, J. The microstructural study of a damaged motorcycle gear wheel. *Manuf. Technol.* **2021**, *21*, 83–90. [CrossRef]
5. Hren, I.; Michna, Š.; Novotný, J.; Michnová, L. Comprehensive analysis of the coated component from a FORD engine. *Manuf. Technol.* **2021**, *21*, 464–470. [CrossRef]
6. Yanase, K.; Endo, M. Multiaxial high cycle fatigue threshold with small defects and craks. *Eng. Mech.* **2014**, *123*, 182–196.
7. He, X.; Wang, M.; Hu Ch Xu, L. Study of the relationship among total oxygen, inclusions and fatigue properties of gear steel. *Mater. Sci. Eng. A* **2021**, *827*, 14199. [CrossRef]
8. Wang, Z.; Xing, Z.; Wang, H.; Shan, D.; Huang, Y.; Xu, Z.; Xie, F. The relationship between inclusions characteristic parameters and bending fatigue performance of 20Cr2Ni4A gear steel. *Int. J. Fatigue* **2022**, *155*, 106594. [CrossRef]
9. Roiko, A.; Hänninen, H.; Vuorikari, H. Anisotropic distribution of non-metallic inclusions in forged steel roll and its influence on fatigue limit. *Int. J. Fatigue* **2012**, *41*, 158–167. [CrossRef]
10. Lipiński, T.; Ulewicz, R. The effect of the impurities spaces on the quality of structural steel working at variable loads. *Open Eng.* **2021**, *11*, 233–238. [CrossRef]
11. Spriestersbach, D.; Grad, P.; Kerscher, E. Influence of different non-metallic inclusion types on the crack initiation in high-strength steels in the VHCF regime. *Int. J. Fatigue* **2014**, *64*, 114–120. [CrossRef]
12. Lipiński, T.; Wach, A.; Detyna, E. Influence of large non-metallic inclusions on bending fatigue strength hardened and tempered steels. *Adv. Mater. Sci.* **2015**, *15*, 33–40. [CrossRef]
13. Zhao, Y.; Li, T.; Tang, G.; Gup, H.; Yan, J.; Gou, X.; Zhu, Y. Characterization of the morphological evolution of MnS inclusions in free-cutting steel during heating. *J. Mater. Res. Technol.* **2022**, *17*, 1427–1437. [CrossRef]
14. Lipiński, T.; Wach, A. The effect of fine non-metallic inclusions on the fatigue strength of structural steel Terms and conditions. *Arch. Metall. Mater.* **2015**, *60*, 65–69. [CrossRef]
15. Guo, Y.; Chen, F.; Liu, B.; Yu, H.; Deng, H. Effect of stress ratio and evaluation of crack sizes on very-high-cycle-fatigue crack propagation life prediction of carburized Cr-Ni steel. *Metals* **2022**, *12*, 1485. [CrossRef]

16. Li, Z.; Zhou, S.; Yang, C.; Yong, Q. High/very high cycle fatigue behaviors of medium carbon pearlitic wheel steels and the effects of microstructure and non-metallic inclusions. *Mater. Sci. Eng. A* **2019**, *764*, 138208. [CrossRef]
17. Lipiński, T.; Wach, A. Influence of outside furnace treatment on purity medium carbon steel. In Proceedings of the METAL 2014—23rd International Conference on Metallurgy and Materials, Brno, Czech Republic, 21–23 May 2014; pp. 738–743.
18. Ulewicz, R.; Szataniak, P.; Novy, F.; Trsko, L.; Bokuvka, O. Fatigue characteristics of structural steels in the gigacycle region of loading. *Mater. Today Proc.* **2017**, *4*, 5979–5984. [CrossRef]
19. Beretta, S.; Murakami, Y. Largest-extreme-value distribution analysis of multiple inclusion types in determining steel cleanliness. *Metall. Mater. Trans.* **2001**, *32B*, 517–523. [CrossRef]
20. Anderson, C.W.; Shi, G.; Atkinson, H.V.; Sellars, C.M. The precision of methods using the statistics of extremes for the estimation of the maximum size of inclusions in clean steels. *Acta Mater.* **2000**, *48*, 4235–4246. [CrossRef]
21. Jonšta, P.; Jonšta, Z.; Brožová, S.; Ingaldi, M.; Pietraszek, J.; Klimecka-Tatar, D. The effect of rare earth metals alloying on the internal quality of industrially produced heavy steel forgings. *Materials* **2021**, *14*, 5160. [CrossRef]
22. Lipiński, T. Effect of the spacing between submicroscopic oxide impurities on the fatigue strength of structural steel. *Arch. Metall. Mater.* **2015**, *60*, 2385–2390. [CrossRef]
23. Blikharskyy, Y.; Selejdak, J.; Kopiika, N. Corrosion fatigue damages of rebars under loading in time. *Materials* **2021**, *14*, 3416. [CrossRef] [PubMed]
24. Milovanovi'c, V.; Duni´c, V.; Raki´c, D.; Živkovi'c, M. Identification causes of cracking on the underframe of wagon for containers transportation—Fatigue strength assessment of wagon welded joints. *Eng. Fail. Anal.* **2013**, *31*, 118–131. [CrossRef]
25. Halford, G.L. *Low Cycle Thermal Fatigue*; NASA: Washington, DC, USA, 1986.
26. Shi, Z.Y.; Li, J.J.; Zhang, X.D.; Shang, C.J.; Cao, W.Q. Influence mechanisms of inclusion types on rotating bending fatigue properties of SAE52100 bearing steel. *Materials* **2022**, *15*, 5037. [CrossRef] [PubMed]
27. Lipiński, T.; Wach, A. Dimensional structure of non-metallic inclusions in high-grade medium carbon steel melted in an electric furnace and subjected to desulfurization. *Solid State Phenom.* **2015**, *223*, 46–53. [CrossRef]
28. Zhang, L.; Pluschkell, W. Nucleation and growth kinetics of inclusions during liquid steel deoxidation. *Ironmak Steelmak* **2003**, *30*, 106–110. [CrossRef]
29. Murakami, Y.; Kodama, S.; Konuma, S. Quantitative evaluation of effects of non-metallic inclusions on fatigue strength of high strength steels, I: Basic fatigue mechanism and fatigue fracture stress and the size and location of non-metallic inclusions. *Int. J. Fatigue* **1989**, *11*, 291–298. [CrossRef]
30. Srivastava, A.; Ponson, L.; Osovski, S.; Bouchaud, E.; Tvergaard, V.; Needleman, A. Effect of inclusion density on ductile fracture toughness and roughness. *J. Mech. Phys. Solids* **2014**, *63*, 62–79. [CrossRef]
31. Hua, L.; Deng, S.; Han, X.; Huang, S. Effect of material defects on crack initiation under rolling contact fatigue in a bearing ring. *Tribol. Int.* **2013**, *66*, 315–323. [CrossRef]
32. Lipiński, T. The effect of the diameter and spacing between impurities on the fatigue strength coefficient of structural steel. *Arch. Metall. Mater.* **2018**, *63*, 519–524.
33. Gulyakov, V.S.; Vusikhis, A.S.; Kudinov, D.Z. Nonmetallic oxide inclusions and oxygen in the vacuum_jet refining of steel. *Steel Transl.* **2012**, *42*, 781–783. [CrossRef]
34. Podorska, D.; Drożdż, P.; Falkus, J.; Wypartowicz, J. Calculations of oxide inclusions composition in the steel deoxidized with Mn, Si and Ti. *Arch. Metall. Mater.* **2006**, *51*, 581–586.
35. Dobrzański, L.A. Heat treatment as the fundamental technological process of formation of structure and properties of the metallic engineering materials. In Proceedings of the 8th Seminar of the International Federation for Heat Treatment and Surface Engineering IFHTSE, Dubrovnik-Cavtat, Croatia, 12–14 September 2001; pp. 1–12.
36. Chan, K.S. Roles of microstructure in fatigue crack initiation. *Int. J. Fatigue* **2010**, *32*, 1428–1447. [CrossRef]
37. Dhua, S.K.; Amitava, R.; Sen, S.K.; Prasad, M.S.; Mishra, K.B.; Jha, S. Influence of nonmetallic inclusion characteristics on the mechanical properties of rail steel. *JMEPEG* **2000**, *9*, 700–709. [CrossRef]
38. Lipiński, T.; Wach, A. Influence of inclusions on bending fatigue strength coefficient the medium carbon steel melted in an electric furnace. *Prod. Eng. Arch.* **2020**, *26*, 86–91. [CrossRef]
39. Dong, Z.; Qian, D.; Yin, F.; Wang, F. Enhanced impact toughness of previously cold rolled high-carbon chromium bearing steel with rare earth addition. *J. Mater. Eng. Perform.* **2021**, *30*, 8178–8187. [CrossRef]
40. Qayyum, F.; Umar, M.; Elagin, V.; Kirschner, M.; Hoffmann, F.; Guk, S.; Prahl, U. Influence of non-metallic inclusions on local deformation and damage behavior of modified 16MnCrS5 steel. *Crystals* **2022**, *12*, 281. [CrossRef]
41. Gu, C.; Liu, W.Q.; Lian, J.H.; Bao, Y.P. In-depth analysis of the fatigue mechanism induced by inclusions for high-strength bearing steels. *Int. J. Miner. Metall. Mater.* **2021**, *28*, 826–834. [CrossRef]
42. Yang, Z.G.; Zhang, J.M.; Li, S.X.; Li, G.Y.; Wang, Q.Y.; Hui, W.J.; Weng, Y.Q. On the critical inclusion size of high strength steels under ultra-high cycle fatigue. *Mater. Sci. Eng. A* **2006**, *427*, 167–174. [CrossRef]
43. Melander, A.; Rolfsson, M.; Nordgren, A.; Jansson, B.; Hedberg, H.; Lund, T. Influence of inclusion contents on fatigue properties of SAE-52100 bearing steels. *Scand. J. Metall.* **1991**, *20*, 229–244.
44. Wang, Y.H.; Yang, Z.N.; Zhang, F.C.; Qin, Y.M.; Wang, X.B.; Lv, B. Microstructures and properties of a novel carburizing nano-bainitic bearing steel. *Mat. Sci. Eng. Struct.* **2020**, *777*, 139086. [CrossRef]

45. Ossola, E.; Pagliassotto, S.; Rizzo, S.; Sesana, R. Microinclusion and fatigue performance of bearing rolling elements. In *Mechanical Fatigue of Metals: Experimental and Simulation Perspectives*; Springer: Berlin/Heidelberg, Germany, 2019; Volume 7, pp. 321–326.
46. Zhou, D.G.; Fu, J.; Chen, X.C.; Li, J. Study on oxygen content, inclusions and fatigue properties of bearing steels produced by different processes. *J. Univ. Sci. Technol. Beijing* **2001**, *8*, 25–27.
47. Mousavi, S.M.; Paavola, J. Analysis of a cracked concrete containing an inclusion within homogeneously imperfect interface. *Mech. Res. Commun.* **2015**, *63*, 1–5. [CrossRef]
48. Lipiński, T.; Pietraszek, J.; Wach, A. Influence of oxygen content in medium carbon steel on bending fatigue strength. In Proceedings of the 21st International Scientific Conference Engineering For Rural Development Proceedings, Jelgava, Latvia, 25–27 May 2022; Volume 21, pp. 351–356.
49. Gu, C.; Lian, J.; Bao, Y.; Münstermann, S. Microstructure-based fatigue modelling with residual stresses: Prediction of the microcrack initiation around inclusions. *Mater. Sci. Eng. A* **2019**, *751*, 133–141. [CrossRef]
50. Macek, W.; Szala, M.; Trembacz, J.; Branco, R.; Costa, J. Effect of non-zero mean stress bending-torsion fatigue on fracture surface parameters of 34CrNiMo6 steel notched bars. *Prod. Eng. Arch.* **2020**, *26*, 167–173. [CrossRef]
51. Lipiński, T. Influence of non-metallic inclusions on bending fatigue strength of high-quality carbon constructional steel heated in an industrial electric arc furnace. *Materials* **2022**, *15*, 6140. [CrossRef]
52. Zhang, G.; Zhang, Q.; Yang, J.; Xie, Z.; Zhang, L.; Liu, R.; Li, G.; Wang, H.; Fang, Q.; Wang, X. Microstructures and tensile properties of 9Cr-f/m steel at elevated temperatures. *Materials* **2022**, *15*, 1248. [CrossRef]
53. Zhang, L.; Ren, Q.; Duan, H.; Ren, Y.; Chen, W.; Cheng, G.; Yang, W.; Sridhar, S. Modelling of non-metallic inclusions in steel. *Miner. Process. Extr. Metall.* **2020**, *129*, 184–206.
54. Ling, H.; Zhang, L.; Li, H. Mathematical modeling on the growth and removal of non-metallic inclusions in the molten steel in a two-strand continuous casting tundish. *Metall. Mater. Trans. B* **2016**, *47*, 2991–3012. [CrossRef]
55. Kocańda, S. *Fatigue Failure of Metals*; WNT: Warsaw, Poland, 1985. (In Polish)
56. *PN-74/H-04327*; Metals Testing for Fatigue. Axial Tensile-Compression Test at a Constant Cycle of External Loads. 1974.